We are IntechOpen,
the world's leading publisher of
Open Access books
Built by scientists, for scientists

4,800

Open access books available

122,000

International authors and editors

135M

Downloads

Our authors are among the

154

Countries delivered to

TOP 1%

most cited scientists

12.2%

Contributors from top 500 universities

CLARIVATE ANALYTICS
BOOK CITATION INDEX
INDEXED

WEB OF SCIENCE™

Selection of our books indexed in the Book Citation Index
in Web of Science™ Core Collection (BKCI)

Interested in publishing with us?
Contact book.department@intechopen.com

Numbers displayed above are based on latest data collected.
For more information visit www.intechopen.com

Heat Transfer in the Environment: Development and Use of Fiber-Optic Distributed Temperature Sensing

Francisco Suárez[1], Mark B. Hausner[1],
Jeff Dozier[2], John S. Selker[3] and Scott W. Tyler[1]
[1]University of Nevada, Reno,
[2]University of California, Santa Barbara,
[3]Oregon State University,
United States

1. Introduction

In the environment, heat transfer mechanisms are combined in a variety of complex ways. Solar radiation warms the atmosphere, the oceans, and the earth's surface, driving weather and climate (Lean & Rind, 1998). Clouds and aerosols reflect a fraction of the incoming solar radiation and partially absorb the infrared radiation that comes from the earth's surface, allowing the existence of acceptable temperatures for the biota and human survival (Norand, 1920; Moya-Laraño, 2010). In water bodies, absorption and scattering of solar radiation results in stratification of the water column (Branco & Torgersen, 2009). Cooling conditions, e.g., convective night-time cooling, at the water surface can destroy the stratification and thus, mix the water column (Henderson-Sellers, 1984). In open water bodies solar radiation also induces evaporation: as water changes its phase, heat is transferred from the water body into the atmosphere by the release of latent heat (Brutsaert, 1982). Within the earth, temperature increases with depth. The temperature at the earth's center is estimated to be on the order of 6000 °C (Alfe et al., 2002). An average geothermal gradient of 25-30 °C km^{-1} (Fridleifsson et al., 2008) indicates that approximately 40 TW (4 × 10^{13} W) flow from the earth's interior to its surface (Sclater et al., 1981). Much of this heat is the result of radioactive decay of potassium, uranium, and thorium (Lee et al., 2009). In the shallow subsurface, this geothermal gradient can be disturbed by groundwater flow and atmospheric conditions (Uchida et al., 2003; Bense & Kooi, 2004).

By measuring the temperature in the environment, it is possible to elucidate the main heat transfer mechanisms controlling different environmental, ecological, geological or engineering processes. Many of these processes span spatial scales from millimeters to kilometers. This extreme range of spatial scaling has been a barrier limiting observation, description, and modeling of these processes. In the past, temperature measurements have been performed at small scales (spanning millimeters, centimeters, or a few meters) or at large scales (spanning tens of meters or kilometers (Alpers et al., 2004)). However, for spatial scales between these two disparate scales and in a variety of media, there is a lack of

methods that can accurately estimate temperatures. Fiber-optic distributed temperature sensing (DTS) is an approach available to provide coverage in both space and time that can be used continuously to monitor real-time data in different environments and at spatial scales that range from centimeters to kilometers. DTS was first developed in the mid 1980s (Dakin et al., 1985) and used in the oil and gas industry during the 1990s and early 2000s (Kersey, 2000), but only since the middle of this decade have DTS instruments achieved acceptable levels of spatial and temporal resolution, along with the high temperature accuracy and resolution needed to observe environmental processes. With their spatial and temporal coverage, DTS methods offer significant advantages over traditional measurement systems in the environment. For instance, the fiber-optic cables that serve as the temperature probe are low cost, with no issues of bias or fluid column disturbance, and variability due to different sensors and sensor measurement scale can be avoided.

The objective of this chapter is to provide the reader with an overview of the theory of fiber-optic DTS technology and a review of environmental applications to date, which will be used to investigate the main heat transfer mechanisms occurring in different environments. Important considerations, recent advances, and future trends are also discussed.

2. Fiber-optic distributed temperature sensing theory

Fiber-optic DTS technology uses Raman spectra scattering in an optical fiber to measure temperature along its length, i.e., the fiber-optic cable is the thermometer, achieving temperature resolutions as small as ±0.01 °C, and spatial and temporal resolutions of 1-2 m and 1-60 s, respectively, for cables up to 10 km (Selker et al., 2006a). Raman scattering can also be used to estimate temperatures in media other than optical fibers, such as atmospheric LIDAR (Eichinger et al., 1993), but can only be used to measure atmospheric temperatures and are far less widely used. To understand how fiber-optic DTS systems work, we first present the background of Raman scattering, describing how this scattering can be used to determine temperatures along the length of the optical fiber. Then, we present the governing equations that DTS systems use.

To measure the temperature along an optical fiber, the DTS instrument emits laser pulses at a known wavelength into an optical fiber. An optical fiber consists of a glass core surrounded by a glass cladding with a different refractive index than the core (Fig. 1). As light travels longitudinally along the fiber, a fraction of the incident light is scattered by interactions between the light and the crystalline structure, and vibration frequency (temperature) of the fiber itself (Hausner, 2010). Light scattering is classified as elastic or inelastic. Elastic (or Rayleigh) scattering occurs when the kinetic energy of the incident photons is conserved and thus, the frequency of the scattered photons is equal than that of the incident light. On the other hand, when the kinetic energy of the incident photons is not conserved, inelastic scattering occurs. As a result, the frequency of the incident and scattered photons differs. In optical fibers, the inelastic scattering typically has two components: Brillouin and Raman. The Brillouin scattering propagates as acoustic waves and is the result of density shifts caused by interaction between pulsed and continuous light waves counter-propagating in the optical fiber (Kurashima et al., 1990). Brillouin scattering occurs at a predictable amplitude but variable frequency. The Raman scattering is produced by interactions between the photons and vibrating molecules within the lattice of the glass fiber. This interaction results in a predictable frequency shift. The scattered light shifted to lower frequencies (longer wavelengths) than the incident light is termed Stokes, while the

scattered light shifted to higher frequencies (shorter wavelengths) is called anti-Stokes. The backscattered Stokes signal is produced when a photon excites a molecule at a base vibrational state and the molecule returns to a slightly higher state (Fig. 2(b)). When the incident photon hits a previously-excited molecule and this molecule returns to the base state (Fig. 2(c)), the backscattered anti-Stokes signal is generated. The greater the temperature of the fiber, the more frequently these previously-excited molecules will be encountered (Smith & Dent, 2005).
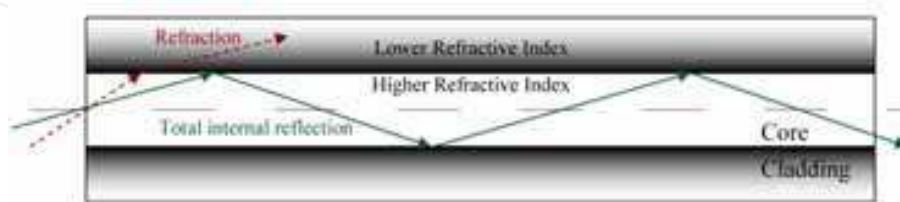

Fig. 1. Internal refractions of light in a cross section of an optical fiber
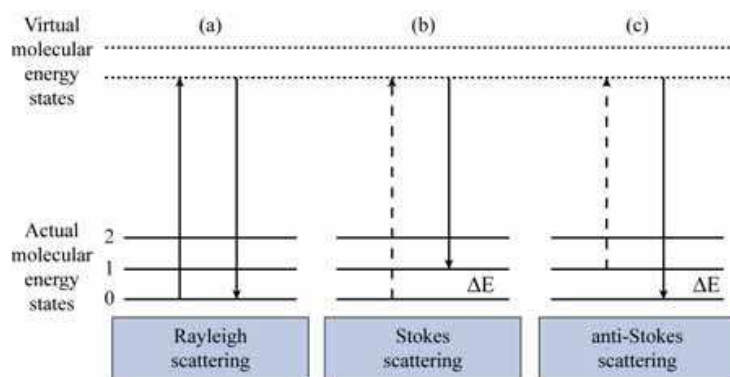

Fig. 2. Interactions between light and glass structure (Smith & Dent, 2005)

Although the frequencies of the Raman signals are predictable, their intensities are not. The intensity of the anti-Stokes scattering depends strongly on the temperature of the silica molecules of the fiber, while the intensity of the Stokes backscattering depends weakly on this temperature (Fig. 3). Because of this differential temperature dependence, the ratio of the anti-Stokes and Stokes signals can be used to determine the temperature of the fiber at the point of scattering (this is described below). The distance of the point of light scatter is calculated by time-domain reflectometry using the speed of light in the glass fiber, which is dependent on the frequency of the light and the index of refraction of the fiber itself. In standard optical fibers, the speed of light ranges between 1.7×10^8 and 2.0×10^8 m s^{-1} (Hausner, 2010). Commercial DTS instruments typically use a 10 or 20 ns laser pulse to illuminate the optical fiber. After emitting the laser pulse, the backscattered signals begin to return to the DTS instrument, where they are collected in discrete time periods by the detector unit. Because the light in the fiber travels approximately 2 m in 10 ns, the signals that return to the DTS instrument between the 0-10 ns following the injected pulse come from the first meter of fiber. If the backscattering detection unit is set to 10 ns, the DTS instrument will return temperature readings integrated over 1 m of fiber. The DTS instrument repeats the pulse and data collection continuously for temporal integration periods as specified by the user. A diagram of a typical DTS system is depicted in Fig. 4.
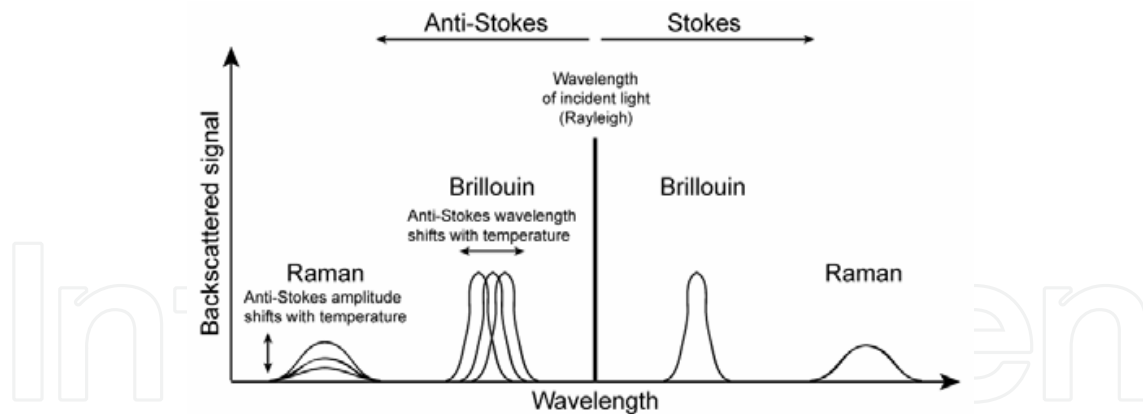
Fig. 3. Diagram of Rayleigh, Brillouin, and Raman backscattering in optical fibers
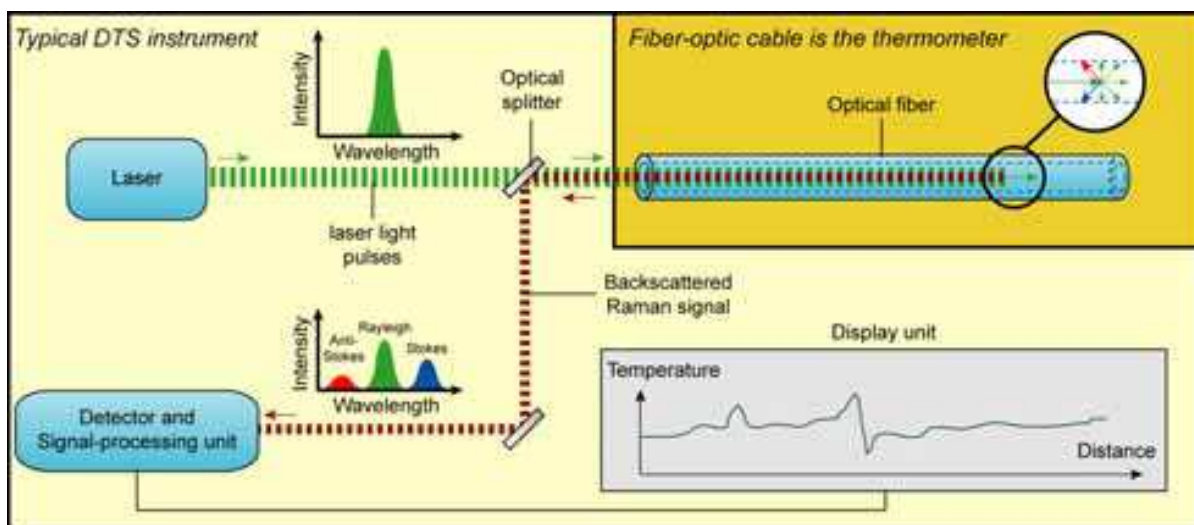

Fig. 4. Diagram of a typical distributed-temperature-sensing system

The intensities of the Raman anti-Stokes and Stokes signals collected at the DTS instrument can be expressed by (Rogers, 1999):

$$I_{aS}(z) = I_0 \exp(-\alpha_0 z)\exp(-\alpha_{aS}z)\wp_{aS}\Gamma_{aS} \tag{1}$$

$$I_S(z) = I_0 \exp(-\alpha_0 z)\exp(-\alpha_S z)\wp_S\Gamma_S \tag{2}$$

where $I_{aS}(z)$ and $I_S(z)$ are the Raman anti-Stokes and Stokes signals, respectively; I_0 is the intensity of the laser pulse emitted from the DTS instrument; α_0, α_{aS} and α_S are the attenuation coefficients of the emitted laser pulse, the backscattered anti-Stokes signal and the backscattered Stokes signal, respectively; $\wp_{aS}$ and $\wp_S$ are the Bose-Einstein probability distribution of phonons of the Raman anti-Stokes and Stokes signals; and Γ_{aS} and Γ_S are the capture coefficients of the Raman anti-Stokes and Stokes signals, which represent the fraction of the scattered light that is directed back towards the light source. The term "$\exp(\alpha_0)$" in equations (1) and (2) represents the attenuation of the emitted light as it travels away from the DTS instrument. The terms "$\exp(\alpha_{aS})$" and "$\exp(\alpha_S)$" represent the attenuation of the anti-Stokes and Stokes signals, respectively, as light travels back into the

DTS instrument. These attenuations are different because the Raman backscattered signals have different frequencies. The Bose-Einstein probability distribution of phonons can be described by (Farahani & Gogolla, 1999):

$$\wp_{aS} = \left[\exp\left(-\frac{\Delta E}{kT}\right) \right]\left[1 - \exp\left(-\frac{\Delta E}{kT}\right) \right]^{-1} \tag{3}$$

$$\wp_{S} = \left[1 - \exp\left(-\frac{\Delta E}{kT}\right) \right]^{-1} \tag{4}$$

where ΔE represents the difference in molecular energy states that drive Raman scattering; k is the Boltzmann constant; and T is absolute temperature. Substituting equations (3) and (4) into equations (1) and (2), respectively, and taking the ratio between the anti-Stokes and Stokes intensities, $R(z)$, yields:

$$R(z) = \frac{I_{aS}(z)}{I_S(z)} = \frac{\Gamma_{aS}}{\Gamma_S} \exp\left(-\frac{\Delta E}{kT}\right)\frac{\exp(-\alpha_{aS}z)}{\exp(-\alpha_S z)} \tag{5}$$

The ratio between the anti-Stokes and Stokes capture coefficients, Γ_{aS}/Γ_S, can be considered as a calibration parameter, C, that depends on the wavelength and frequency of the incident laser, the backscattered Raman signals, the instrument's photon detector, and the operating conditions of the DTS instrument. Defining the differential attenuation of the backscattered Stokes and anti-Stokes as $\Delta\alpha = \alpha_S - \alpha_{aS}$ and $\gamma = \Delta E/k$, equation (5) results in:

$$R(z) = C\exp\left(-\frac{\gamma}{T}\right)\exp(\Delta\alpha z) \tag{6}$$

and rearranging terms (Suárez et al., 2011):

$$T(z) = \frac{\gamma}{\ln[C] - \ln\left[R(z)\right] + \Delta\alpha z} \tag{7}$$

Equation (7) describes the temperature along the entire optical fiber. Here, for the sake of simplicity, the differential attenuation has been assumed to be constant along the fiber but in reality, this may change along the fiber due to differences in manufacturing, strain or other defects that scatter the two Stokes frequencies differently. From equation (7), it can be seen that integrated measurements of temperature, in both space and time, along the fiber can be estimated using the ratio of the anti-Stokes and the Stokes intensities. As explained before, when determining the temperature along the optical fiber, the location of the point of scatter must also be known. This location can be found by measuring the duration of the light reflection in the optical fiber. The distance, z, traveled by the light can be estimated by (Yilmaz & Karlik, 2006):

$$z = \frac{ct}{2n} \tag{8}$$

where c is the speed of light in vacuum, n is the refractive index of the fiber, and t is the propagation time of light in the forward and backward directions. More details about the

theoretical basis of DTS system can be found in other investigations (Rogers, 1999; Selker et al., 2006a).

3. Use of fiber-optic distributed temperature sensing in the environment

The use of fiber-optic DTS in the environment began during the 1990s (Hurtig et al., 1994; Förster et al., 1997) when temperature in boreholes was monitored with resolutions of ±0.1 °C. In the middle of the 2000s, DTS systems achieved acceptable levels of spatial and temporal resolution, along with high temperature accuracy and resolution to monitor the environment. For example, when the systems are calibrated carefully, using integration times longer than 1 h and cables shorter than 5 km, a precision of ±0.01 °C can be achieved every 1 meter of cable (Selker et al. 2006a,b). This great ability to precisely observe temperatures at thousands of locations is the main thrust of DTS systems, which holds potential for transformative observation of many environmental processes. In this section, we present an overview of the DTS applications that have been performed in different environments. To show the promise of this technology, we present hydrological, ecological, engineering, and atmospheric DTS applications that have been studied.

3.1 Fiber-optic distributed temperature sensing in snow

Measurement of the thermal regime of snow has significant importance to a wide range of environmental processes, yet can be surprisingly challenging to measure. Snow depth and snow temperature strongly control the thermal balance and temperature profiles in the underlying soil (Lachenbruch, 1959) as well as heat transfer between the snow and atmosphere. The vertical distribution of temperature strongly controls metamorphism in the snowpack, important for both avalanche forecasting and snowmelt dynamics. In addition, the horizontal variation of snow temperatures can control the distribution of permafrost and frozen ground, both important factors for infiltration, runoff and many sub-snow biological processes. However, in almost all cases, snow temperature measurements are limited to one or at most a few points of measurement in space across the landscape.

While temperature sensing systems have been available for centuries, snow represents several unique challenges. In the past, measurements were often made by hand in snow pits, using simple thermometers but providing, at best, a very limited time series of the temperature evolution. Even with advances in continuous, low-cost, low-power thermal data collectors (Lundquist & Lott, 2008), measurements of the thermal regime of snow packs are still generally limited to a few points in the vertical dimension, and rarely more than a few different locales in any given watershed. Even continuous vertical measurements are challenging, as solar radiation and wind often cause melting, heat conduction and/or differential snow accumulation around measurement devices. The lack of ability to measure, continuously in time and space, the snow thermal environments has limited our understanding of the energy budgets of snow covered areas, as well as the spatial distribution of snow physical properties. Recently, Tyler et al. (2008) demonstrated the utility of DTS for measuring the thermal evolution of the snow/soil interface temperatures. In that work, standard telecommunication cables were deployed across several hundred meters at two experimental watersheds and monitored to determine the thermal differences between snow and bare ground, and also the effects of aspect on soil/snow interface temperatures. In both watersheds, deployed fibers withstood winter conditions and

provided 300-400 individual measurements of snow/soil interface temperatures at temporal scales from minutes to hours (Tyler et al., 2008).

Since basal snow temperatures are now proven to be easily measured using DTS, the distribution of internal snowpack temperatures represents the next challenge in distributed sensing. While it has long been recognized that vertical gradients in the snowpack temperature lead to significant snow metamorphosis and instability, little study has been made on the horizontal gradients in temperature that may exist due to differences in shading and snow accumulation. Areas of steep horizontal gradient in snow temperatures may result in horizontal differences in vapor diffusion, snow morphology and strength, thereby producing local zones of weakness that may serve as avalanche trigger points.

Several methods have been proposed in the last few years to measure internal snowpack temperatures using fiber-optic sensing in harsh conditions during winter and snow loading. Researchers from École Polytechnique Fédérale de Lausanne and Oregon State University have suspended and stretched fiber-optic cables at fixed elevations above the soil prior to the onset of winter, and allowed the fiber-optic "fence" to be subsequently buried by snow. Such a design provides temperature data at fixed elevations above the land surface and precise knowledge of the cable location. Challenges to the fixed height method include cable sagging due to snow load, stress points at any cable attachment point and alteration of the snow deposition due to the presence of the pre-emplaced cable "fence". Alternatively, optical fiber can be deployed as snow accumulates during the winter season and allowed to follow both the snow surface, and any compaction/consolidation that occurs. Researchers at the University of Nevada, Reno and the University of California, Santa Barbara have used this deployment strategy in the Sierra Nevada of California, where storm accumulations are typical large and quickly bury the deployed fiber, and access to the site allows for easy deployment prior to major storms. Far less precise spatial location (both horizontal and depth) can be predicted for this method, as the optical fiber is deployed before the storm cycle begins, the optical fiber can move due to wind during the storm, and blowing snow may bury the cable differentially. Following the storm, the optical fiber should remain at the interface of the old and new snow, but its height above the ground surface will decrease as the snow consolidates through the season. This method of deployment therefore tracks snow layer temperatures, rather than at fixed depths in the snowpack. While there is potentially less strain on the fiber due to attachment points and less effect of the cable placement on snow accumulation, both methods are likely to alter the snow melting dynamics as the optical fiber approaches the snow surface during the melt season. While the "snow fence" method requires significant work at the beginning of the season, the "pre-storm" deployment requires significant work throughout the snow season and repeated access to the study site.

At the CRREL-UCSB Eastern Sierra Snow Study Site (CUES, Painter et al., 2000; Bales et al., 2006), fiber-optic DTS monitoring of basal and snowpack temperatures has been on-going since 2007 (Tyler et al., 2008). During the 2009/2010 and 2010/2011 winter seasons, fiber-optic cable (ADSS Flat Drop Cable, AFL Telecommunications, Duncan, SC) was deployed across the CUES field site to measure internal snowpack temperatures. Prior to the first snow, fiber-optic cable was deployed, including a 70m loop of cable south of the instrument shelter, and three coils of approximately 70m of fiber to be deployed during the winter season. Beginning on February 4, 2010, these coils were deployed on the snow surface over one another on successive storms (February 4, 21, and March 2, respectively). The snow depths at these times, as measured by an ultrasonic sounder, were 40 cm, 270 cm and

approximately 350 cm, respectively. Throughout the winter season, DTS temperature measurements were made (Sensornet Halo, Sensornet Inc., Hertfordshire, UK) using 1 minute averaging intervals and post-processed using instrumented calibration baths (Tyler et al., 2008).
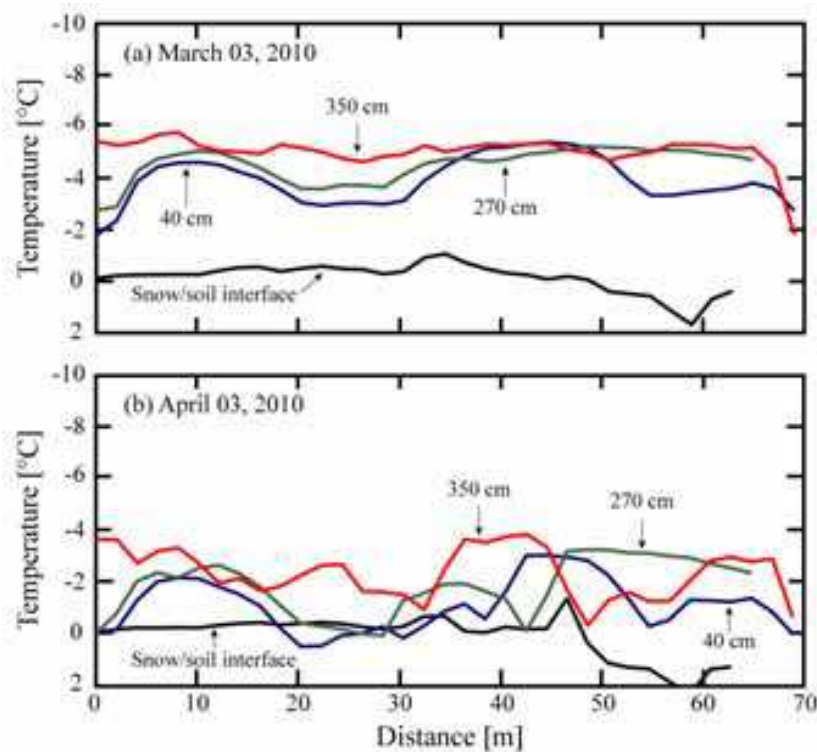

Fig. 5. (a) Horizontal distribution of snowpack temperatures from the CUES site on March 3, 2010. The elevations shown in the figures represent initial position of the fiber. Note that significant horizontal variation in temperature is visible in the 40 and 270 cm cables.
(b) Horizontal distribution of snowpack temperatures from the CUES site later in the season (April 3, 2010) shows much warmer snowpack as well as smaller vertical gradients in snow temperature. Horizontal differences continue to remain along each depth, and remain fixed in space when compared to the March 3, 2010 data

Fig. 5 (a) shows the temperature distribution from the soil surface up through the snowpack along the 70 meters of instrumented snow (Note that the y-axis is reversed to place the uppermost coil, which is also the coldest, at the highest elevation in the snowpack). Vertical thermal gradients, assuming the initial snow depths as representative lengths, range from 0.3 to approximately 8 °C m^{-1}. Horizontal gradients are also quite apparent (maximum ~0.25 °C m^{-1}), particularly in the 40 and 270 cm cables where two zones of colder conditions can be seen between 5 and 20 m and, to a lesser degree, between approximately 35 and 55 m. Both of these locations correspond with areas of snow ablation, with the zone between them characterized by drifted snow. Fig. 5 (b) shows the same transect data from one month later in the season (April 3, 2010). Snow temperatures are generally warmer, with much smaller differences with depth. However, horizontal differences have persisted, and remain stationary. At this time, vertical gradients have decreased to near zero in some areas, while the horizontal gradients reach a maximum of approximately 1 °C m^{-1}. Based upon visual observation of the transect late in the season, the zones of largest horizontal gradients

correspond to rapid changes in snow depth, i.e., between drifts. In these zones, since the fiber-optic cable follows snow interfaces, the zones of coldest measurement correspond to areas of shallowest snow, where the fiber-optic cable is closer to the snow/air interface. While the horizontal gradients are small, their persistence and their gain in importance compared to the vertical gradient late in the snow season suggest that they may have significance in late season snow melt and snow stability. These transitions in temperature may lead to melt enhancement as well as serve as locations of weakness that could result in avalanche triggers on the slopes in the same area. Such horizontal variations in snow temperature are rarely recognized from individual snow pits or profiles and point to the utility of fiber-optic DTS approaches for snow thermal measurement.

The use of DTS for snow thermal process monitoring is relatively new and shows significant progress. Applications to snowmelt dynamics and frozen ground analysis are already underway and provide unique remotely sensed data that are important for hydrologic and environmental monitoring. Progress has been made in snowpack internal temperature measurement, and preliminary data suggest that horizontal gradients in snow temperature become significant late in the season as snowpacks approach melting conditions. Using fiber-optic DTS provides the first and only reliable method in which the spatial variability of snowpack temperatures can easily and remotely be measured. Measurement of both vertical and horizontal gradients and their spatial variability may provide important insights into snowpack dynamics, melting and avalanche susceptibility.

3.2 Fiber-optic distributed temperature sensing in ecohydrology

Devils Hole, a geothermally influenced groundwater-filled fracture in the carbonate aquifer of the southern Mojave Desert, represents a unique intersection of geology, hydrology, and ecology. The system offers a window into the carbonate aquifer of the Death Valley regional flow system (Riggs & Deacon, 2002), and is home to the world's only extant population of the endangered Devils Hole pupfish (*Cyprinodon diabolis*). Thought to comprise the smallest habitat containing the entire population of a vertebrate species (Moyle, 2002), Devils Hole was severely impacted by the development of nearby groundwater resources in the 1960s and early 1970s (Andersen & Deacon, 2001), leading to extensive litigation that to this day influences the United States' management of endangered species and water resources (Riggs & Deacon, 2002). The scientific footprint of Devils Hole is as significant as its legal impact; the system has been the site of pioneering work in palaeoclimate reconstructions (Winograd et al., 2006), as well as ichthyology (Minckley & Deacon, 1973) and evolution (Miller, 1950; Lema & Nevitt, 2006). In the late 1990's, the population of *C. diabolis* experienced an unexplained decline that has only recently stabilized, and a number of the hypotheses to explain this decline posit changes to the physical habitat of the system, especially changes in water temperatures.

Cyprinodon species tend to be very sensitive to water temperatures, and the 33-34 °C waters in Devils Hole are near the upper tolerance of most species (Brown & Feldmeth, 1971). The reproductive cycle of this fish is particularly temperature-dependent, and oogenesis in adult females, the viability of fertilized eggs, and the development of hatched larvae can all be severely retarded by exposure to higher temperatures (Shrode & Gerking, 1977). The thermal tolerances of *Cyprinodon* species also appear to be related to the variability of the water temperatures in which they live (Otto & Gerking, 1973) – the Devils Hole pupfish, which lives its entire life in water is seldom outside 33-35 °C, is especially susceptible to thermal stresses. Because the population of *C. diabolis* varies seasonally from highs of 200 to

lows of fewer than 70 individuals, small variations in water temperature can have enormous impacts on the health of the population as a whole. Over the last three years, researchers have been using DTS instrumentation to characterize the thermal regime of Devils Hole.

Devils Hole comprises a 3 m x 8 m shallow shelf, which provides a spawning ground for the pupfish population, and a deep pool with a surface area of barely 30 m². The fracture that forms the deep pool strikes NE-SW and dips approximately 70°, with a uniform aperture of approximately 4 m. Between the surface and a depth of 30 m, the system is approximately 15 m wide along the NE-SW axis; below 30 m it opens into a cavern approximately 100 m wide, although the 4 m aperture remains. Devils Hole has been explored by divers to a depth of 130 m, and the clear waters allow visibility to almost 150 m (Riggs & Deacon, 2002). Below that point, the structure of the system is unknown. In January 2009, a fiber-optic cable was permanently installed in the deep pool to observe vertical temperature profiles.
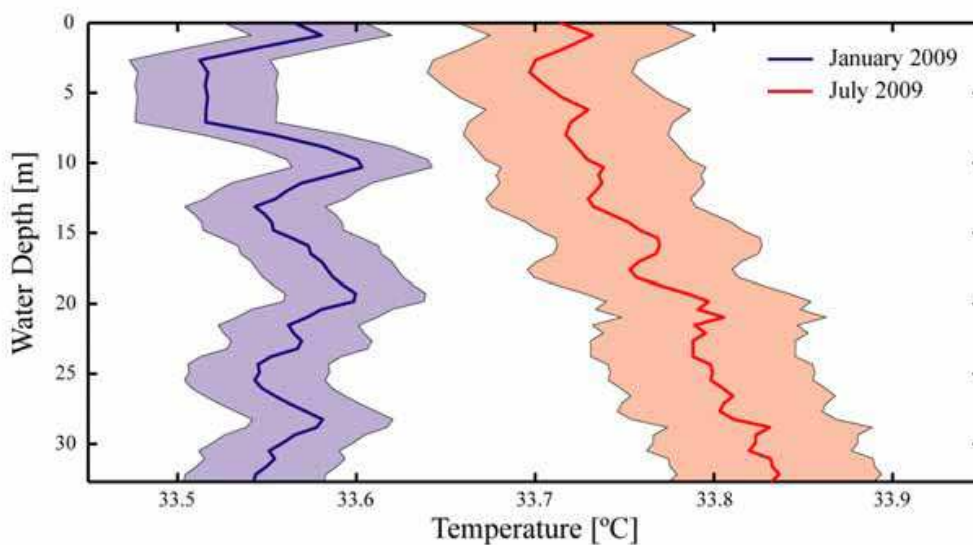

Fig. 6. Seasonal changes in the vertical temperature profiles of Devils Hole. The heavy lines indicate the mean temperature over 48 hours, and the shaded areas indicate the root mean square error of the calibrated DTS data (0.04° and 0.06° C in January and July, respectively)

Hausner et al. (2010) presented seasonal changes in the vertical temperature profiles that revealed a previously unidentified cycle of convective mixing. Fig. 6 shows the vertical temperature profiles observed in January and July, 2009. The near-uniform temperatures in the January profile indicate a system in which convective mixing is the dominant mode of heat transfer, while the constant temperature gradient observed in July fits a system dominated by conduction. In the summer, the water on the surface is warm, and tends to remain at the surface; the waters below the surface are warmed and stabilized by the natural geothermal gradient in the area, and the inverted temperature profile results. When water on the shallow shelf cools in the winter, the greater density causes it to plunge through the stratified water below, and the system mixes. The seasonal mixing affects the oxygen dynamics of the system, the winter distribution of allochthanous carbon (one of the pupfish's primary sources of food), and the availability of nutrients in the water column. However, these patterns would likely not have been noticed without the use of DTS in Devils Hole. This mixing model is based on observations of temperature gradients as small as 0.005 °C m⁻¹. Because a single common calibration is used to return DTS temperature

observations along the entire length of the cable, fine gradients such as the one shown in Fig. 6 can be more easily observed and more confidently quantified with DTS instruments than with traditional sensors. Using a thermistor string, for example, the summer temperature gradient shown in Fig. 6 would likely have been lost in the noise generated by comparing multiple, separately calibrated instruments.

3.3 Fiber-optic distributed temperature sensing in salt-gradient solar ponds

A salt-gradient solar pond is a non-traditional solar collector that can provide long-term thermal storage and recovery for the collected energy. It is an artificially stratified water body that consists of three distinct zones (Suárez et al., 2010a): the upper convective zone, which is a thin layer of cooler and fresher water; the non-convective zone, comprised of a salt-gradient to suppress global circulation within the pond; and the lower-convective zone, in which salinity and temperature are the highest. The solar radiation that reaches the bottom of the pond is transformed into thermal energy and warms the brine in the lower convective zone. This warmer brine cannot rise beyond the lower convective zone because the effect of salinity on density is greater than the effect of temperature. The heat stored in the lower convective zone can only escape to the atmosphere by conduction, making the thickness of the non-convective zone a critical operating parameter for efficient solar pond operation (Suárez et al., 2010b). Because the brine has a low thermal conductivity, heat losses by conduction are relatively small. The hot brine in the lower convective zone may then be used directly for heating (Rabl and Nielsen, 1975), thermal desalination (Lu et al., 2001; Suárez et al., 2010c), or for other low-temperature thermal applications (Kumar and Kishore, 1999).

To investigate sustainable freshwater production using thermal desalination powered with solar energy, Suárez et al. (2010a, 2011) constructed a 1.0-m depth experimental salt-gradient solar pond. The pond was built inside a laboratory operated under controlled conditions, and was initially exposed to artificial lights 12 h per day. After reaching a thermal quasi steady-state, the pond was exposed continuously to the artificial lights until a new thermal steady-state was reached. Then, heat was extracted at approximately 0.5 m depth and was used to drive membrane distillation (Suárez, 2010). This pond was instrumented with a variety of sensors, including a vertical high-resolution DTS system to accurately monitor the thermal stratification and to investigate thermohaline circulation. This vertical high-resolution DTS system was constructed by wrapping a fiber-optic cable around a polyvinyl chloride pipe of approximately 1.3 m in length. This allowed temperature measurements every 1.1 cm in the vertical direction. A detailed explanation of the experimental salt-gradient solar pond and the characteristics of the vertical high-resolution DTS system are presented by Suárez et al. (2011).

Fig. 7 (a) presents the thermal evolution of the experimental salt-gradient solar pond as measured by the vertical high-resolution DTS system. Over the 15-days of the maturation period, the brine of the lower convective zone (0.65 m to 1.0 m) was warmed approximately 18 °C and showed strong internal convection when the lights were on. When the lights were off, the lower convective zone stratified due to the heat lost through the bottom and sides of the pond as well as through the non-convective zone. The upper convective zone (0.0 m to 0.1 m) also showed a diurnal pattern of strong stratification (due to radiation absorption) and subsequent mixing at night (due to penetrative convective mixing) during the first week of the experiment. After this, the upper convective zone showed strong internal convection during the day and night. This occurred because of the higher temperatures in the non-

convective zone, which warms the bottom of the upper convective zone and induce thermal convection cells in this zone. On the other hand, the non-convective zone (0.1 m to 0.65 m) showed only conductive heat transfer effectively isolating the warm layer below. The data collected using the vertical high-resolution DTS system also allowed closing of the energy budget in this rather unique thermohaline environment. Tyler et al. (2009a) estimated the sensible heat flux (Fig. 7 (b)) at the surface of the pond by measuring the net radiation (at the water surface), estimating the evaporation rate over the pond, and combining these measurements with the change in heat storage in the pond, which was evaluated using the DTS system.
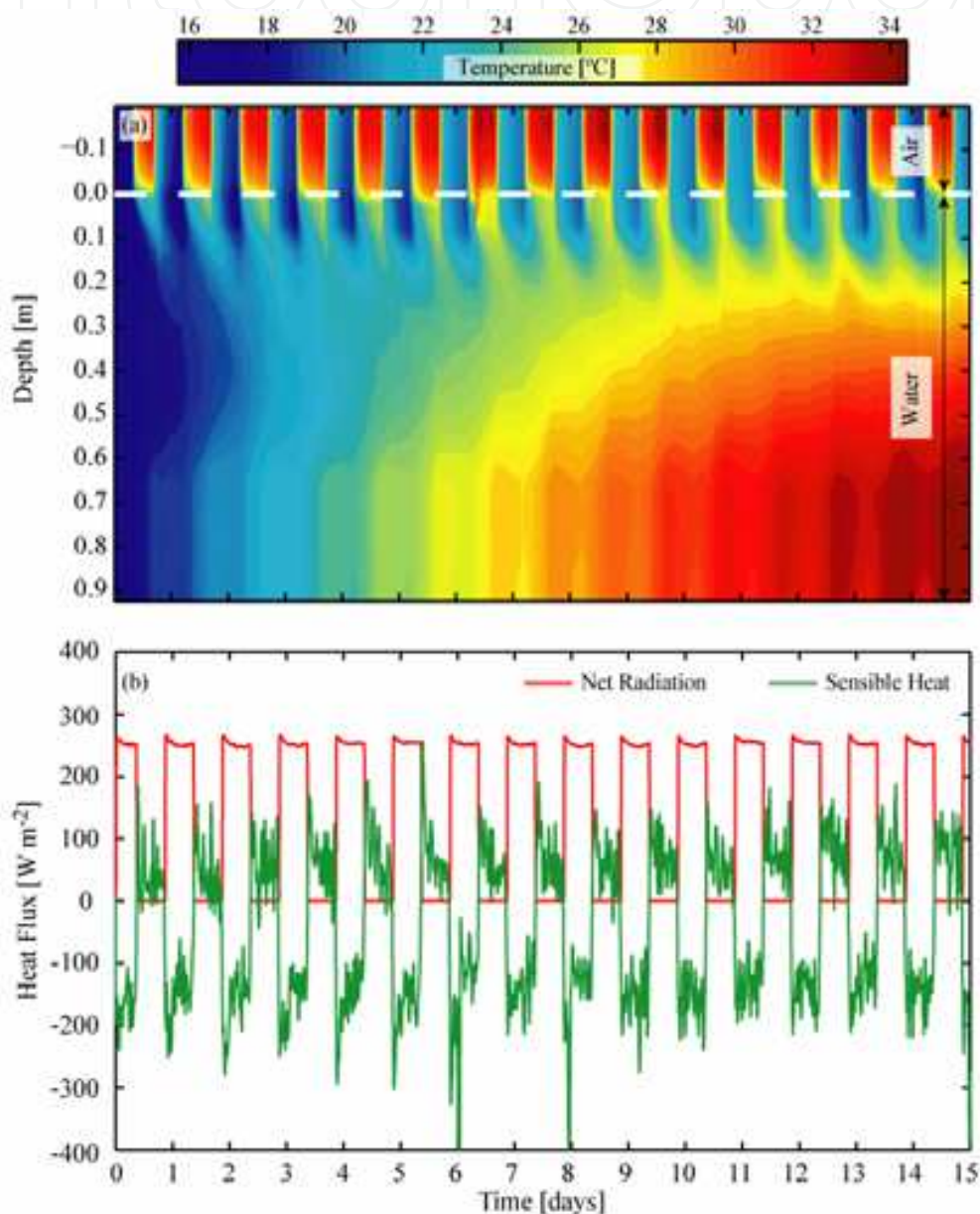

Fig. 7. (a) Thermal evolution of the water column and the air above it in an experimental salt-gradient solar pond as measured by a vertical high-resolution fiber optic distributed-temperature-sensing system (Suárez et al., 2011). (b) Heat fluxes at the surface of the pond were calculated by closing the energy balance (Tyler et al., 2009a)
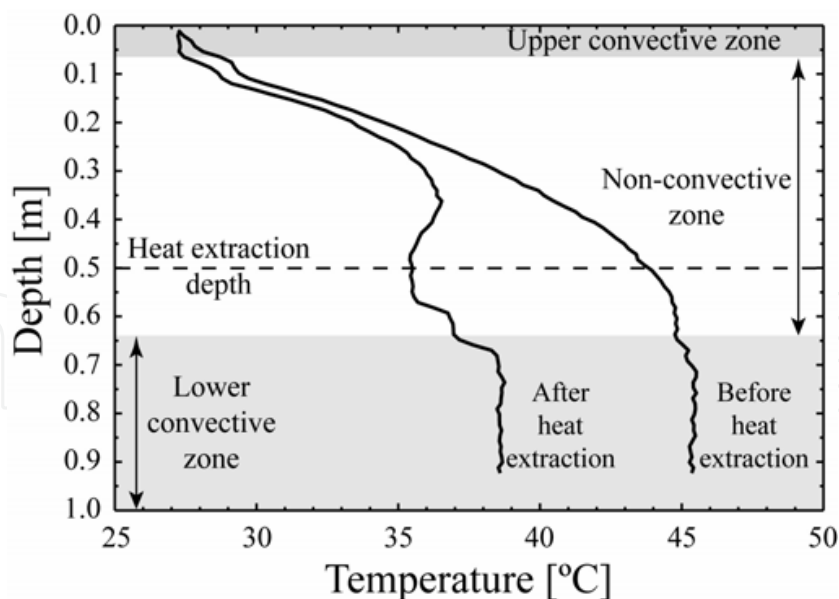
Fig. 8. Temperature profile in the salt-gradient solar pond at the beginning and at the end of a heat extraction experiment. Modified from Suárez et al. (2010a)

Suárez et al. (2010a) also presented results of heat extraction in the experimental salt-gradient solar pond. As shown in Fig. 8, before heat was extracted from the pond, the temperature in the lower convective zone was approximately 45 °C and the lower portion of the non-convective zone was completely mixed (between 0.55 and 0.65 m). The temperature step change of 0.5 °C observed in the interface between these zones suggests that transport is occurring by double-diffusive convection (Turner, 1974). Fig. 8 also shows that heat was extracted directly from the non-convective zone and indirectly from the lower convective zone. As heat was extracted, the temperature at the heat extraction depth decreased, and when it was cooler than a threshold, the fluid at this depth sank to the bottom of the pond. As a result, the warmer brine from the lower convective zone rose and energy was now extracted from this brine. After 45 hours of heat extraction, the temperature profile showed a staircase shape below the heat extraction depth. This staircase is typical of double-diffusive convective systems (Kelley et al., 2003) and occurred inside the salt-gradient solar pond because of the method used to create the salt-gradient within the pond (Suárez et al., 2010a).

3.4 Detection of illicit connections in storm water sewers

Storm water sewer systems discharge rain or storm waters into surface waters without treatment. Illicit connections that introduce fouled water in storm water systems are very problematic because they result in the release of untreated sewage in surface water bodies such as rivers, lakes or even the sea. Recently, Hoes et al. (2009a) developed a searching technique for detection of illicit connections in storm water system using DTS. Monitoring the temperature in storm water sewers allows finding anomalous temperatures or temperature variations at the illicit connections. Typically, the sewer temperatures are influenced by surrounding air, soil, and sometimes by the temperatures of other types of waters that enters the sewer (Dürrenmatt & Wanner, 2008). Temperatures in an approximate range between 5 and 20 °C are expected for sewer conditions, and the variations within this range can only occur on a daily and seasonal basis. On the other hand, domestic wastewater

usually shows a broader variation. For example, houses appliances and showers heat domestic waters, and temperatures in the range 30–90 °C could be expected in the drain. Even though the temperature drops as the domestic water travels before discharging into the sewer system, temperatures warmer than 20 °C could be found at the illicit connection (Hoes et al., 2009a).

Fig. 9 shows the DTS measurements performed by Hoes et al. (2009a) at an illicit connection that was located using this new technique. The temperatures in the sewer were relatively stable at approximately 12 °C, especially during the night. During the day and evening, anomalous peaks of temperatures were observed at this specific location. On-site verification by excavation and testing provided conclusive evidence that these temperature anomalies resulted from illicit connections in the storm water system.
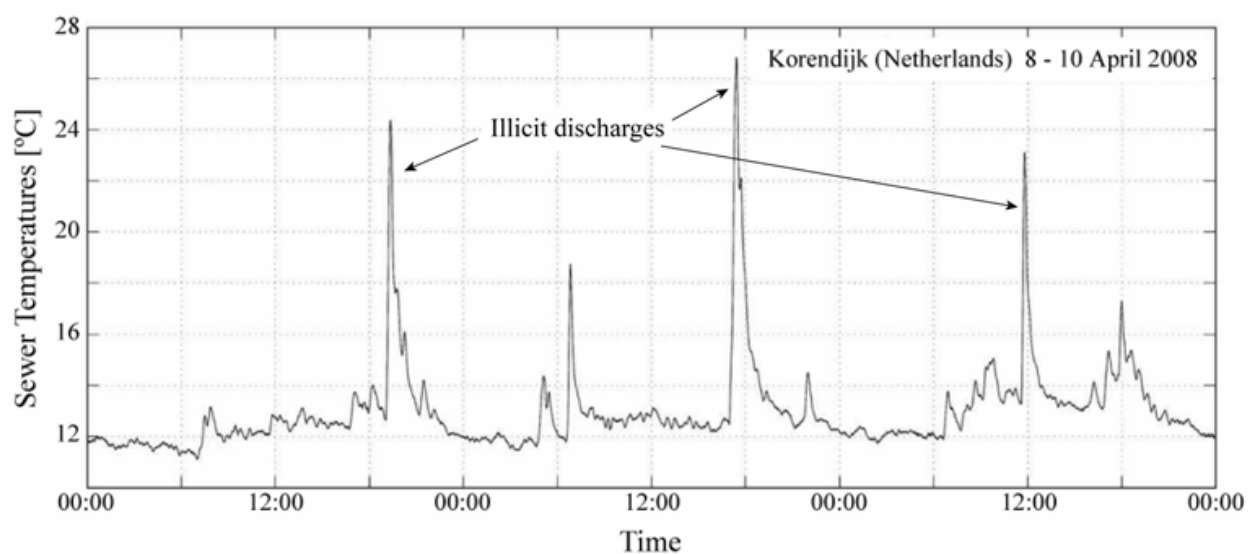

Fig. 9. DTS measurements performed in Korendijk (Netherlands) at the location of an illicit connection of a storm water system. Modified from Hoes et al. (2009a)

3.5 Distributed temperature sensing as an indirect tool for soil moisture estimation

Soil moisture is a key-state variable in water and energy balances at the land surface, and affects many different physical and environmental processes. The water content of a given soil is a controlling factor for agriculture and crop production, biological activity within the soil microbial community, and meteorological processes (Hausner, 2010). It also influences how efficiently water and solutes can move through the soil matrix. Despite its widespread influence and importance, measuring soil moisture is a difficult task, especially at field scale when soil heterogeneity could be important. The spatial scales of water content measurements present additional challenges. At small scales, single point measurements can be taken at specific intervals. However, these measurements are typically expensive, time consuming, and are difficult to extrapolate to field scale (e.g., over areas larger than 0.1 km^2). Remote sensing technologies can estimate near-surface soil moisture over larger areas, but there is a lack on methods to estimate in-situ water content at scales ranging from 0.1 to 80 km^2 (Robinson et al., 2008). By burying fiber-optic cables and recording the spatial distribution of soil temperatures over several days, Steele-Dunne et al. (2010) demonstrated that DTS can be used to estimate the distribution of soil moisture within these spatial scales. They first described heat transfer in a soil column using the diffusion equation:

$$\frac{\partial T}{\partial t} = D(\theta)\frac{\partial^2 T}{\partial z^2} = \frac{\kappa(\theta)}{C(\theta)}\frac{\partial^2 T}{\partial z^2} \tag{8}$$

where T is temperature; t is time; θ is volumetric water content (or soil moisture); $D(\theta)$, $\kappa(\theta)$ and $C(\theta)$ are the thermal diffusivity, thermal conductivity, and thermal heat capacity of the bulk soil, respectively, which are each functions of soil moisture; and z is depth. By measuring temperature at different depths, the soil thermal properties can be inferred by inversion, then the soil moisture can be estimated using a representative relationship between the soil thermal conductivity and soil moisture. Steele-Dunne et al. (2010) chose the Campbell exponential model (Campbell, 1985):

$$\kappa(\theta) = a + b\theta - (a-d)\exp\left[-(c\theta)^e\right] \tag{9}$$

where a, b, c, d and e are empirical parameters that depend on the volume fraction of soil minerals (e.g., quartz), organic matter, and on the clay fraction.

Steele-Dunne et al. (2010) buried two fiber-optic cables at approximately 8 and 10 cm below the surface of the ground to monitor the thermal response of the diurnal signal. A section of approximately 50 m was used to measure the transient temperature field at each depth and soil moisture was derived from these measurements. Even though they obtained reasonable results for both the soil thermal diffusivity and relative saturation (Fig. 10), it must be pointed out that their method relies on knowledge of the depth of the cable, and small variations were shown to cause large errors in the estimation of the thermal properties of the soil and thus, in the estimated values of soil moisture. The key of this method is the linkage between soil moisture and soil temperatures. Thus, the relationship between soil moisture and soil thermal conductivity must also be ascertained using in situ measurements over the entire range of saturation values (Steele-Dunne et al., 2010).
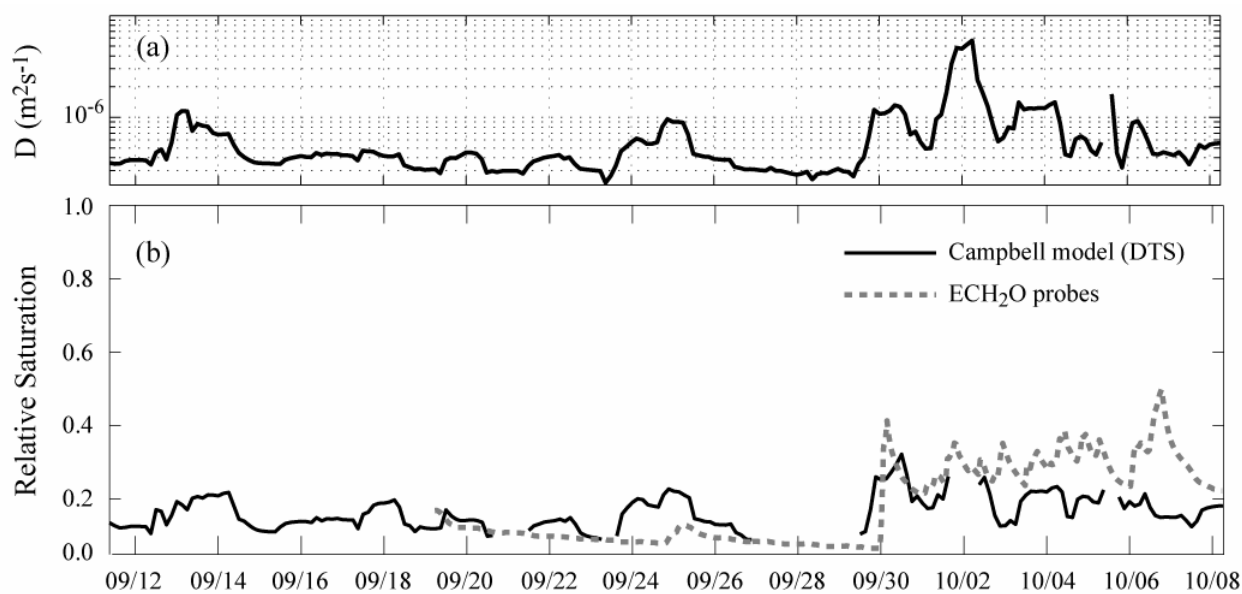

Fig. 10. (a) Estimated thermal diffusivity (D) at a selected location along the fiber-optic cable. (b) Mean value of relative saturation observed using ECH$_2$O probes and inferred relative saturation from the estimated thermal diffusivity using the Campbell model (1985). Modified from Steele-Dunne et al. (2010)

Sayde et al. (2010) also demonstrated the feasibility of using DTS to obtain accurate distributed measurements of soil water content. While Steele-Dunne et al. (2010) made passive observation of the natural diurnal cycles of heating and cooling, Sayde et al. (2010) actively heated a fiber-optic cable that was buried in variably saturated sand and then correlated the cumulative temperature increase and dissipation at different depths with the corresponding soil water content. Their correlations showed coefficients of determination (R^2) higher than 0.985, showing the promise of this method. Current efforts on spatially distributed soil moisture estimation are trying to combine both the passive and active DTS methods to obtain more precise measurements at field scale.

3.6 Atmospheric boundary layer estimation using distributed temperature sensing

The atmospheric boundary layer height, also called the mixed-layer or mixing height, is the lower part of the atmosphere in which the influence of heating and cooling, and surface friction is important (Brutsaert, 1982). The vertical mixing that occurs in this layer is driven by turbulence produced primarily by wind shear and buoyancy. The height of the atmospheric boundary layer is a key parameter for describing the physical state of the lower troposphere because it allows the prediction of air pollution concentrations or surface temperatures. For instance, air pollutants emitted at the ground surface will mix into this layer and, depending on meteorological conditions, can reach elevations from meters to a few kilometers (Brutsaert, 1982; Keller et al., 2011). Although it is one of the main parameters in atmospheric applications, the weakest point in meteorology is still the determination of the atmospheric boundary layer height (Builtjes, 2001).
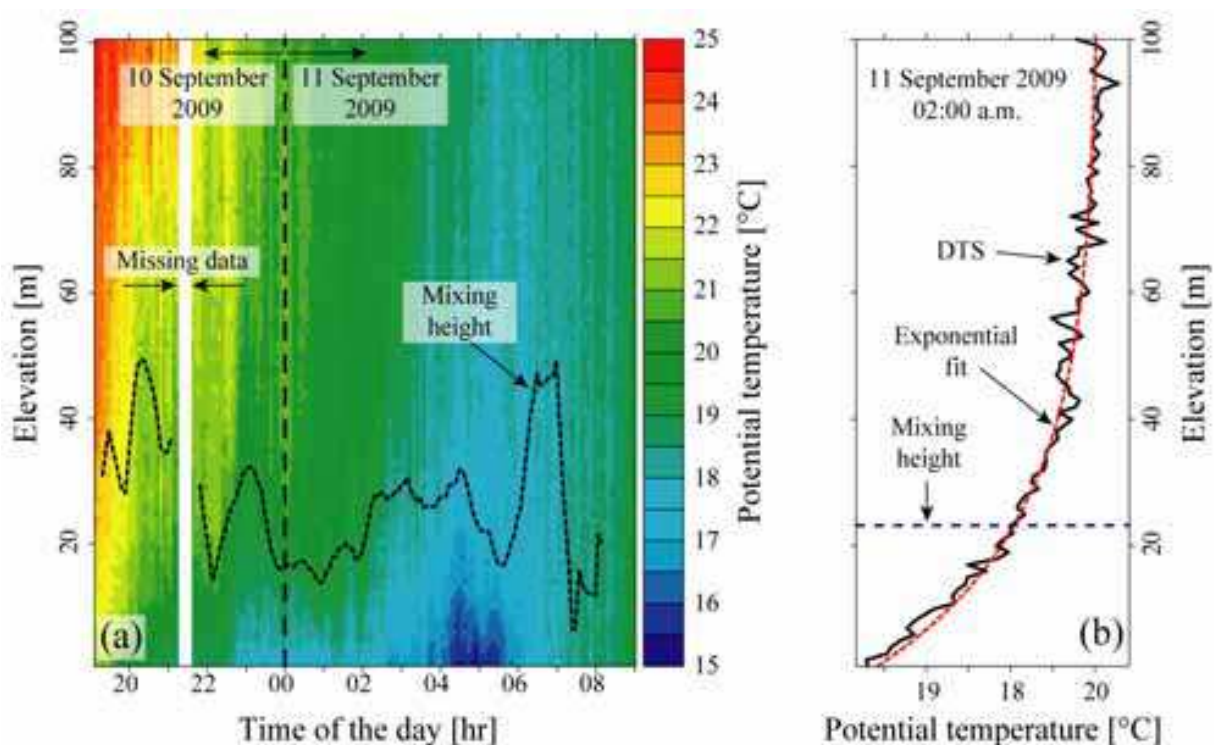

Fig. 11. (a) Evolution of potential temperature in the lowest 100 m of the atmosphere and mixing height as determined from exponential profile fits (bold-dashed line). (b) Example of a thermal profile measured by the DTS system with the corresponding best fit of an exponential curve. The mixing height is also shown. Modified from Keller et al. (2011)

Keller et al. (2011) presented a new method for measuring the air temperature profiles in the atmospheric boundary layer. A tethered balloon lifting system was used to suspend the optical fiber in the lowest 100 m of the atmosphere. As shown in Fig. 11, the temperature data were used to estimate the height of the stable boundary layer during the night, which varied between 5 and 50 m (September 11th data). They were also able to observe the erosion of the stable atmospheric stratification that occurred shortly after sunrise when the surface warmed. This resulted in an increase of turbulence, convection, and mixing due to latent and sensible heat being transferred to the atmosphere.

3.7 Other applications of fiber-optic distributed temperature sensing

Since it is difficult to describe all the work that has been carried out using this technology, in this section we present a brief summary of other environmental applications that were not described before.

Surface water-groundwater exchange has been widely studied using DTS methods in different environments such as estuaries (Henderson et al., 2009), rivers and streams (Lowry et al., 2007; Westhoff et al., 2007; Vogt et al., 2010; Slater et al., 2010), and ditches and canals (Hoes et al., 2009b). In general, these applications have used DTS technology to identify gaining sections of rivers, i.e., sections of the river where groundwater enters into it. The exception is the work of Vogt et al. (2010), where a vertical high-resolution DTS system was installed to measure both stream and streambed-sediment temperatures, which also allowed the estimation of the seepage rates from the river into the groundwater. Other environmental applications related with stream dynamics include the processes that controls thermal regime of saltmarsh channel beds (Moffett et al., 2008), development of distributed stream temperature models (Westhoff et al., 2007), response of stream temperatures in different riparian vegetation (Roth et al., 2010), and quantification of heat retardation along streams (Westhoff et al., 2010). The effects of radiative heating on fiber-optic cables used to monitor water temperatures have also been evaluated (Neilson et al., 2010; Suárez et al., 2011).

Early DTS work in hydrogeology was focused on thermal monitoring of geothermal wells and boreholes (Hurtig et al., 1994; Förster et al., 1997). Then, DTS systems were used to analyze the dynamic subsurface thermo-hydraulic conditions in aquifers (Macfarlane et al., 2002). Recently, Freifeld et al. (2008) developed a methodology to determine thermal conductivity in boreholes by combining a fiber-optic DTS system with a resistance heater, which created a controlled thermal perturbation in the borehole. The transient thermal data is inverted to estimate the thermal conductivity profile along the length of a wellbore with a spatial resolution equal to the spatial resolution of the DTS instrument. They also were able to determine the baseline geothermal profile and the ground surface temperature history in their study site (High Lake region, Nunavut, Canada).

4. Important considerations and future trends

Even though DTS systems have significant advantages over traditional measurement systems (as shown above), they also have limitations that must be assessed to maximize the potential of this technology. The performance of a DTS system is highly dependent upon the design of the experiment, the DTS instrument, the fiber-optic cables and connectors, the calibration, and the operating conditions. In this section we briefly discuss these factors in order to obtain thermal measurements with improved accuracy and precision.

4.1 Distributed-temperature-sensing instruments

There are a wide variety of commercial DTS instruments that use different methods for signal generation and data processing, which will affect the resolution and cost of the system. The cost of a DTS instrument ranges from approximately $15,000 to more than $150,000 (April 2011 U.S. Dollars). This cost depends on the features of each system (e.g., spatial and temporal resolution, ports to connect external thermocouples, number of channels). For temporary installations, there is also the option to lease DTS instruments for a lower cost (Tyler and Selker, 2009). The power requirements for DTS instruments range from approximately 20 to more than 100 W. To select the most cost-effective system, the required temporal and spatial repeatability must be evaluated by taking into account the goals and characteristics of each installation. The temporal and spatial averaging need to be long enough to provide suitable temperature resolutions, but short enough to observe the transient phenomena and the physics behind the system that is being measured.

4.2 Fiber-optic cables and connectors

As the cable acts as a thermometer, the selection of the cable is crucial in the experimental design. The cable typically includes a plastic jacket, tensile strength members, armoring to protect the optical fiber, a water-tight barrier, and the optical fiber(s). The cost of the cable can range from approximately $0.5 m^{-1} to more than $10 m^{-1} and cable weights can range from <1 kg km^{-1} to more than 30 kg km^{-1}. In general, the cost and weight of the cable are determined more by the armoring and construction than by the optical fiber itself. As cables get heavier, they are more difficult to handle and they can respond more slowly to temperature changes. Localized strains and stresses over the cable can result in greater signal losses, thus it is important to understand the environment of the installation before selecting the cable. Another important factor is the exposure of the cable to solar radiation, especially when used in the atmosphere or in shallow streams. Fiber-optic cables, as well as other thermal sensors, can absorb solar radiation and monitor higher temperatures than those of the surrounding ambient. This issue is more important when air or water velocities are small, and when the magnitude of solar radiation is large (Neilson et al., 2010). The effect of solar radiation absorption on cables can be reduced using reflective coatings or shielding the cable (Suárez et al., 2011). In addition, in a long-term installation with a cable exposed to sunlight, for example, it is important to select jackets that can withstand ultra-violet radiation and that can minimize radiative heating.

Connectors can also have an impact on signal strength. The standard connectors in the DTS industry typically produce a signal loss on the order of 0.1–0.2 dB (or even more if the connector is not clean or is incorrectly aligned). This loss is approximately the same loss that occurs in 300–700 m of fiber-optic cable, respectively (assuming an attenuation of ~0.3 dB km^{-1}). Ideally, the cable should only have connectors to physically connect the cable itself with the DTS instrument. If fibers need to be joined, fusion splices are recommended, since a properly fused fiber splice has a loss on the order of 0.01–0.03 dB.

4.3 Calibration and types of measurements

The calibration process is critical to achieve measurements with high resolution. An optimum deployment should have at least three sections of known temperature, each one with at least 10 sampling points within its length (e.g., 10 m when the spatial sampling resolution is 1 m). As suggested by Suárez et al. (2011), two of these sections can be at the same temperature and the other section needs to be at a different temperature. Ideally, the

known-temperature sections should bracket the expected observations in the corresponding environment. If possible, the fiber-optic cable should have a loop to return the cable to the instrument (see Suárez et al. (2011) for more details about calibration procedures). This permits the DTS instrument to interrogate the fiber-optic from each end, i.e., allowing single- or double-ended measurements. Single-ended measurements refer to temperatures estimated from light transmission in only one direction along the optical fiber. These measurements assume a uniform rate of differential attenuation ($\Delta\alpha$) over the entire fiber, and provide greater precision near the instrument, degrading with distance because of the energy loss along the fiber length. Double-ended measurements refer to temperatures estimated from light transmission in both directions along the optical fiber. In these measurements, the temperature is estimated using single-ended measurements made from each end of the fiber, and can account for spatial variation in the differential attenuation of the anti-Stokes and Stokes backscattered signals, which typically occurs in strained fibers. Double-ended measurement results in a signal noise more evenly distributed across the entire length of the optical fiber, but uniformly greater than that obtained in a single-ended measurement (Tyler et al., 2009b; Suárez et al., 2011). Single-ended calibrations are encouraged for short cables (i.e., smaller than 1 or 2 km) since they provide more precision near the instrument. However, sometimes strains or sharp bends in the deployed fiber-optic cable yields large localized losses in the Stokes and anti-Stokes signals, which decrease the magnitude of the signals and add noise to the temperature data. Because these localized losses cannot be handled adequately by a single uniform value of the differential attenuation, further calibration is sometimes required to translate the scattered Raman signals into usable temperature data. In these cases, double-ended measurements are recommended because they allow the calculation of the differential attenuation along the entire length of the cable, and are much better able to handle the step losses introduced by strains and bends.

4.4 Operating conditions

An issue that has been observed in DTS installations is drift of the instrument. This drift typically occurs because of large variations in the instrument's temperature, particularly when the DTS instrument is subject to large daily temperature fluctuations in the field. The best solution to minimize this drift is to put the instrument in a controlled environment if possible. Other solution to minimize drift is to calibrate the DTS instrument at every measurement (sometimes referred to as dynamic calibration).

4.5 Current and future trends

As previously described, the ability to precisely measure temperature at thousands of locations is the main thrust of DTS systems. This capability has opened a new window for observation of environmental processes. Typical DTS instruments currently used in environmental applications can achieve temperature resolutions as small as ±0.01 °C, and spatial and temporal resolutions of 1-2 m and 10-60 s, respectively. At present, there are ongoing efforts to improve both spatial and temporal resolution of DTS systems. A high-resolution DTS instrument (Ultima, Silixa, Hertfordshire, UK) with temporal and spatial resolutions of 1 Hz and 12.5 cm, respectively, was recently commercialized and is under testing in environmental applications. This instrument simultaneously improved temporal precision by a factor of ten and spatial precision by a factor of four over previously available units. It was first deployed for observation of turbulent and stable atmospheric processes

(http://oregonstate.edu/bmm/DONUTSS-2010/first-deployment-array), and it has also been utilized during a borehole heat tracer experiment designed to identify zones of high horizontal hydraulic conductivity and borehole through-flow. While this new DTS instrument has opened many possibilities, observation of atmospheric processes, for example, still needs improvement of temporal resolution to monitor turbulent processes. Instruments with this improved resolution are expected to be available in the near future and definitively will open new opportunities for observation of environmental processes.

5. Conclusion

In the environment, heat transfer mechanisms are combined in a variety of ways and span spatial scales that range from millimeters to kilometers. This extremely wide spatial scaling has been a barrier that limits observation, description, and modeling of environmental processes. The introduction of fiber-optic DTS has contributed to fill the gap between these two disparate scales. Fiber-optic DTS has proven effective to precisely observe temperatures at thousands of locations at the same time, with no issues of bias, and avoiding variability due to use of different sensors.

In this work, we have shown some of the environmental applications that have benefited from DTS methods. For instance, using fiber-optic DTS provides the first and only reliable method in which the spatial variability of snowpack temperatures can easily and remotely be measured. Measurement of both vertical and horizontal gradients and their spatial variability may provide important insights into snowpack dynamics, melting and avalanche susceptibility. DTS methods also have improved thermal measurements in natural and managed aquatic systems. For example, the hydrodynamic regimes in Devils Hole were observed at resolutions smaller than 0.1 °C, allowing observation of temperature gradients as small as 0.003 °C m^{-1}. This resolution allowed the examination of seasonal oxygen and nutrient distribution in the water column. In salt-gradient solar ponds, this temperature resolution allowed observation of both mixing and stratification, which is important for pond efficiency. In both Devils Hole and the solar pond, fiber-optic DTS provided high-resolution thermal measurements without disturbance of the water column. DTS methods also have been successfully utilized in other environments such as in atmosphere, streams, boreholes, and in many applications to understand the interdependence between groundwater and surface water. Novel extensions of DTS methods include spatially distributed soil moisture estimation, detection of illicit connections in storm water sewers, and there are many more to come in the near future, especially because the technology is growing and improving the spatial and temporal resolutions of DTS instruments, which will open new opportunities for environmental observations.

6. Acknowledgement

7. References

Alfe, D., Gillan, M.J., Vocadlo, L., Brodholt, J. & Price, G.D. (2002). The ab initio simulation of the earth's core. *Philosophical Transaction of the Royal Society of London A,* Vol.360, No.1795, (June 2002), pp. 1227-1244, ISSN 1364–503X

Heat Transfer in the Environment:
Development and Use of Fiber-Optic Distributed Temperature Sensing
631

Alpers, M., Eixmann, R., Fricke-Begemann, C., Gerding, M. & Höffner, J. (2004). Temperature lidar measurements from 1 to 105 km altitude using resonance, Rayleigh, and Rotational Raman scattering. *Atmospheric Chemistry and Physics,* Vol.4, No.3, (2004), pp. 793-800, ISSN 1680-7316

Andersen, M.E & Deacon, J.E. (2001). Population size of Devils Hole pupfish (Cyprindon diabolis) correlates with water level. *Copeia,* Vol.2001, No.1, (February 2001), pp. 224-228, ISSN 0045-8511

Bales, R.C., Molotch, N.P, Painter, T.H, Dettinger, M.D., Rice, R. & Dozier, J. (2006). Mountain hydrology of the western United States. *Water Resources Research,* Vol.42, No.W08432, (2006), 13 pp., ISSN 0043-1397

Bense, V.F. & Kooi, H. (2004). Temporal and spatial variations of shallow subsurface temperature as a record of lateral variations in groundwater flow. *Journal of Geophysical Research,* Vol.109, No. B04103, (2004), 13 pp., ISSN 0148-0227

Branco, B.F. & Torgersen, T. (2009). Predicting the onset of thermal stratification in shallow inland waterbodies. *Aquatic Sciences,* Vol.71, No.1, (March 2009), pp. 65-79, ISSN 1015-1621

Brown, J.H. & Feldmeth, C.R. (1971). Evolution in constant and fluctuating environments: thermal tolerances of desert pupfish (Cyprinodon). *Evolution,* Vol.25, No.2, (June 1971), pp. 390-398, ISSN 0014-3820

Brutsaert, W. (1982). *Evaporation into the atmosphere: theory, history and applications* (1st Edition), Springer, ISBN 9789027712479, London, England

Builtjes, P.J.H. (2001). Major twentieth century milestones in air pollution modelling and its Applications, In: *Air Pollution Modeling and its Applications XIV*, Gryning, S.E. & Schiermeier (eds.), Springer, pp.3-16, Kluwer Academic/Plenum Publishers, ISBN 0306465345, New York

Campbell, G.S. (1985). *Soil physics with BASIC: transport models for soil-plant systems* (3rd Edition), Elsevier, ISBN 9780444425577, New York, USA

Dakin, J.P., Pratt, D.J., Bibby, G.W. & Ross, J.N. (1985). Distributed optical fiber Raman temperature sensor using a semiconductor light-source and detector. *Electronics Letters,* Vol.21, No.13, (1985), pp. 569-570, ISSN 0013-5194

Dürrenmatt, D.J. & Wanner, O. (2008). Simulation of the wastewater temperature in sewers with TEMPTEST. *Water Science and Technology*, Vol.57, No.11, (2008), pp.1809-1815, ISSN 0273-1223

Eichinger, W.E., Cooper, D.I., Parlange, M. & Katul, G. (1993). The Application of a Scanning, Water Raman-Lidar as a Probe of the Atmospheric Boundary Layer. *IEEE Transactions on Geoscience and Remote Sensing,* Vol.31, No.1, (January 1993), pp.70-79, ISSN 0196-2892

Farahani, M.A. & Gogolla, T. (1999). Spontaneous Raman Scattering in Optical Fibers with Modulated Probe Light for Distributed Temperature Raman Remote Sensing. *Journal of Lightwave Technology*, Vol.17, No.8, (August 1999), pp.1379-1391, ISSN 0733-8724

Förster, A., Schrötter, J., Merriam, D.F. & Blackwell, D. (1997). Application of optical-fiber temperature logging—An example in a sedimentary environment. *Geophysics*, Vol.62, No.4, (July-August 1997), pp.1107-1113, ISSN 0016-8033

Fridleifsson, I.B., Bertani, R., Huenges, E., Lund, J.W., Ragnarsson, A. & Rybach, L. (2008). The possible role and contribution of geothermal energy to the mitigation of

climate change, *In: O. Hohmeyer and T. Trittin (Eds.) IPCC Scoping Meeting on Renewable Energy Sources, Proceedings*, pp. 20-25, Luebek, Germany, January 20-25, 2008

Freifeld, B.M., Finsterle, S., Onstott, T.C., Toole P. & Pratt, L.M. (2008). Ground surface temperature reconstructions: using in situ estimates for thermal conductivity acquired with a fiber-optic distributed thermal perturbation sensor. *Geophysical Research Letters*, Vol.35, No.L14309, (2008), 5 pp., ISSN 0094-8276

Hausner, M.B. (2010). *Estimating in situ integrated soil moisture content using fiber-optic distributed temperature sensing (DTS) measurements in the field.* M. Sc. Thesis, University of Nevada, Reno, 124 pp.

Hausner, M.B., Tyler, S.W., Wilson, K.P., Gaines, D.B. & Selker, J.S. (2010). Devils Hole: a window into the carbonate aquifer of the Death Valley regional flow system. *Abstract H31A-0977 presented at 2010 Fall Meeting, American Geophysical Union*, San Francisco, California, USA, December 2010

Henderson, R.D., Day-Lewis, F.D. & Harvey, C.F. (2009). Investigation of aquifer-estuary interaction using wavelet analysis of fiber-optic temperature data. *Geophysical Research Letters*, Vol.36, No.L06403, (2009), 6 pp., ISSN 0094-8276

Henderson-Sellers, B. (1984). *Engineering Limnology* (1st Edition), Pitman Published Limited, ISBN 0273085395, London, England

Hoes, O.A.C, Schilperoort, R.P.S., Luxemburg, W.M.J., Clemens, F.H.L.R. & van de Giesen, N.C. (2009a). Locating illicit connections in storm water sewers using fiber-optic distributed temperature sensing. *Water Research,* Vol.43, No.20, (December 2009), pp. 5187-5197, ISSN 0043-1354

Hoes, O.A.C., Luxemburg, W.M.J., Westhoff, M.C., van de Giesen, N.C. & Selker, J.S. (2009b). Identifying seepage in ditches and canals in polders in the Netherlands by distributed temperature sensing. *Lowland Technology International,* Vol.11, No.2, (December 2009), pp. 21-26, ISSN 1344-9656

Hurtig, E., S. Großwig, S., Jobmann, M., Kühn, K. & Marschall, P. (1994). Fibre-optic temperature measurements in shallow boreholes: experimental application for fluid logging. *Geotermics,* Vol.23, No.4, (August 1994), pp. 355-364, ISSN 0375-6505

Kelley, D.E., Fernando, H.J.S., Gargett, A.E., Tanny, J. & Özsoye, E. (2003). The diffusive regime of double-diffusive convection. *Progress in Oceanography*, Vol.86, No.3-4, (March 2003), pp. 461-481, ISSN 0079-6611

Keller, C.A., Huwald, H., Vollmer, M.K., Wenger, A., Hill, M., Parlange, M.B. & Reimann, S. (2011). Fiber optic distributed temperature sensing for the determination of the nocturnal atmospheric boundary layer height. *Atmospheric Measurement Techniques*, Vol.4, No.2, (2011), pp. 143-149, ISSN 1867-1381

Kersey, A.D. (2000). Optical fiber sensors for permanent downwell monitoring applications in the oil and gas industry. *IEICE Transactions on Electronics,* Vol.E83c, No.3, (March 2000), pp. 400-404, ISSN 0916-8524

Kumar, A. & Kishore, V. (1999). Construction and operational experience of a 6000 m2 solar pond at Kutch, India. *Solar Energy,* Vol.65, No.4, (March 1999), pp. 237-249, ISSN 0038-092X

Kurashima, T., Horiguchi, T. & Tateda, M. (1990). Distributed-temperature sensing using stimulated Brillouin scattering in optical silica fibers. *Optics Letters,* Vol.15, No.18, (1990), pp. 1038-1040, ISSN 0146-9592

Lachenbruch, A.H. (1959). Periodic heat flow in a stratified medium with applications to permafrost problems. U.S. Geological Survey Bulletin, 1083-A, 36 pp.

Lean, J. & Rind, D. (1998). Climate Forcing by Changing Solar Radiation. *Journal of Climate,* Vol.11, No.12, (December 1998), pp. 3069-3094, ISSN 0894-8755

Lee, K.K.M., Steinle-Neumann, G. & Akber-Knutson, S. (2009). Ab initio predictions of potassium partitioning between Fe and Al-bearing $MgSiO_3$ perovskite and post-perovskite. *Physics of the Earth and Planetary Interiors,* Vol.174, No.1-4, (May 2009), pp. 247-253, ISSN 0031-9201

Lema, S.C. & Nevitt, G.A. (2006). Testing an ecophysiological mechanism of morphological plasticity in pupfish and its relevance to conservation efforts for endangered Devils Hole pupfish. *The Journal of Experimental Biology,* Vol.209, No.18, (September 2006), pp. 3499-3509, ISSN 0022-0949

Lowry, C.S., Walker, J.F., Hunt, J.H. & Anderson, M.P. (2007). Identifying spatial variability of groundwater discharge in a wetland stream using a distributed temperature sensor. *Water Resources Research,* Vol.43, No.W10408, (2007), 9 pp., ISSN 0043-1397

Lu, H. , Walton, J. & Swift, A. (2001). Desalination coupled with salinity-gradient solar ponds. *Desalination,* Vol.136, No.1-3, (May 2001), pp. 13-23, ISSN 0011-9164

Lundquist, J.D. & Lott, F. (2008). Using inexpensive temperature sensors to monitor the duration and heterogeneity of snow-covered areas. *Water Resources Research,* Vol.44, No.W00D16, (2008), 6 pp., ISSN 0043-1397

Miller, R.R. (1950). Speciation in fishes of the genera Cyprinodon and Empetrichthys inhabiting the Death Valley region. *Evolution,* Vol.4, No.2, (June 1950), pp. 155-163, ISSN 0014-3820

Minckley, C.O & Deacon, J.E. (1973). Observations on the reproductive cycle of Cyprinodon diabolis. *Copeia,* Vol.1973, No.3, (August 1973), pp. 610-613, ISSN 0045-8511

Moffett, K.B., Tyler, S.W., Torgersen, T., Menon, M., Selker, J.S. & Gorelick, S.M. (2008). Processes controlling the thermal regime of saltmarsh channel beds. *Environmental Science and Technology,* Vol.42, No.3, (January 2008), pp. 671-676, ISSN 0013-936X

Moya-Laraño, J. (2010). Can Temperature and Water Availability Contribute to the Maintenance of Latitudinal Diversity by Increasing the Rate of Biotic Interactions? *The Open Ecology Journal,* Vol.3, No.1, (2010), pp. 1-13, ISSN 1874-2130

Moyle, P.B. (2002). *Inland Fishes of California: Revised and Expanded* (1st edition), University of California Press, ISBN 9780520227545, Berkeley, California, USA

Neilson, B.T., Hatch, C.E., Ban, H. & Tyler, S.W. (2010). Solar radiative heating of fiber-optic cables used to monitor temperatures in water. *Water Resources Research*, Vol.46, No.W08540, (2010), 17 pp., ISSN 0043-1397

Norand, C.W.B. (1920). Effect of High Temperature, Humidity, and Wind on the Human Body. *Quarterly Journal of the Royal Meteorological Society,* Vol.46, No.193, (January 1920), pp. 1-14, ISSN 0035-9009

Otto, R.G. & Gerking, S.D. (1973). Heat tolerance of a Death Valley pupfish (genus Cyprinodon). *Physiological Zoology,* Vol.46, No.1, (January 1973), pp. 43-49, ISSN 0031-935X

Painter, T.H., Donahue, D., Dozier, J., Li, W., Kattelmann, R., Dawson, D., Davis, R.E., Fiori, J., Harrington, B. & Pugner, P. (2000). The Mammoth Mountain cooperative snow study site: data acquisition, management, and dissemination. *Proceedings of the*

International Snow Science Workshop, Vol. ISSW2000, pp. 447-451, Big Sky, Montana, USA, October 2000

Rabl, A. & Nielsen, C. (1975). Solar ponds for space heating. *Solar Energy,* Vol.17, No.1, (April 1975), pp. 1-12, ISSN 0038-092X

Riggs, A. & Deacon, J.E. (2002). Connectivity in Desert Aquatic Ecosystems: The Devils Hole Story, *Proceedings of Spring-fed wetlands: important scientific and cultural resources of the intermountain region*, DHS Publication No. 41210, Las Vegas, Nevada, USA, May 2002, available from: http://www.dri.edu/spring-fed-wetlands

Robinson, D.A., Campbell, C.S., Hopmans, J.W., Hornbuckle, B.K., Jones, S.B., Knight, R., Ogden, F., Selker, J.S. & Wendroth, O. (2008). Soil moisture measurement for ecological and hydrological watershed-scale observatories: a review. *Vadose Zone Journal*. Vol.7, No.1, (February 2008), pp. 358-389, ISSN 1539-1663

Rogers, A. (1999). Distributed optical-fibre sensing. *Measurement Science and Technology,* Vol.10, No.8, (August 1999), pp. R75-R99, ISSN 0957-0233

Roth, T.R., Westhoff, M.C., Huwald, H., Huff, J.A., Rubin, J.F.,Barrenetxea, G., Vetterli, M., Parriaux, A., Selker, J.S. & Parlange, M.B. (2010). Stream Temperature Response to Three Riparian Vegetation Scenarios by Use of a Distributed Temperature Validated Model. *Environmental Science and Technology,* Vol.44, No.6, (February 2010), pp. 2072–2078, ISSN 0013-936X

Sayde, C., Gregory, C., Gil-Rodriguez, M., Tufillaro, N., Tyler, S.W., van de Diesen, N.C., English, M., Cuenca, R. & Selker, J.S. (2010). Feasibility of soil moisture monitoring with heated fiber optics. *Water Resources Research*, Vol.46, No.W06201, (2010), 8 pp., ISSN 0043-1397

Sclater, J.G, Parsons, B. & Jaupart, C. (1981). Oceans and Continents: Similarities and Differences in the Mechanisms of Heat Loss. *Journal of Geophysical Research,* Vol.86, No.B12, (1981), pp. 11535-11552, ISSN 0148-0227

Selker, J.S., Thevenaz, L., Huwald, H., Mallet, A., Luxemburg, W., van de Giesen, N.C., Stejskal, M., Zeman, J., Westhoff, M. & Parlange, M.B. (2006a). Distributed fiber-optic temperature sensing for hydrologic systems. *Water Resources Research,* Vol.42, No.W12202, (2006a), 8 pp., ISSN 0043-1397

Selker, J.S., van de Giesen, N.C., Westhoff, M., Luxemburg, W. & Parlange, M.B. (2006b). Fiber optics opens window on stream dynamics. *Geophysical Research Letters*, Vol.33, No.L24401, (2006), 4 pp., ISSN 0094-8276

Shrode, J.B. & Gerking, S.D. (1977). Effects of constant and fluctuating temperatures on reproductive performance of a desert pupfish, Cyprinodon n. nevadensis. *Physiological Zoology,* Vol.50, No.1, (January 1977), pp. 1-10, ISSN 0031-935X

Slater, L.D., Ntarlagiannis, D., Day-Lewis, F.D., Mwakanyamale, K., Versteeg, R.J., Ward, A., Strickland, C., Johnson, C.D. & Lane, J.W. (2010). Use of electrical imaging and distributed temperature sensing methods to characterize surface water–groundwater exchange regulating uranium transport at the Hanford 300 Area, Washington. *Water Resources Research,* Vol.46, No.W10533, (2010), 13 pp., ISSN 0043-1397

Smith, E. & Dent, G. (2005). *Modern Raman spectroscopy: a practical approach* (1st Edition), John Wiley and Sons, ISBN 978-0471497943, Sussex, England

Steele-Dunne, S.C., Rutten, M.M., Krzeminska, D.M., Hausner, M.B., Tyler, S.W., Selker, J.S., Bogaard, T.A. & van de Giesen, N.C. (2010). Feasibility of Soil Moisture Estimation

Heat Transfer in the Environment:
Development and Use of Fiber-Optic Distributed Temperature Sensing
635

using Passive Distributed Temperature Sensing. *Water Resources Research,* Vol.42, No.W03534, (2010), 12 pp., ISSN 0043-1397

Suárez, F. (2010). *Salt-gradient solar ponds for renewable energy, desalination and reclamation of terminal lakes.* Ph. D. Thesis, University of Nevada, Reno, 195 pp.

Suárez, F., Childress, A.E. & Tyler, S.W. (2010a). Temperature evolution of an experimental salt-gradient solar pond. *Journal of Water and Climate Change*, Vol.1, No.4, (2010), pp. 246-250, ISSN 2040-2244.

Suárez, F., Tyler, S.W. & Childress, A.E. (2010b). A fully coupled transient double-diffusive convective model for salt-gradient solar ponds. *International Journal of Heat and Mass Transfer*, Vol.53, No.9-10, (April 2010), pp. 1718-1730, ISSN 0017-9310.

Suárez, F., Tyler, S.W. & Childress, A.E. (2010c). A theoretical study of a direct contact membrane distillation system coupled to a salt-gradient solar pond for terminal lakes reclamation. *Water Research*, Vol.44, No.15, (August 2010), pp. 4601-4615, ISSN 0043-1354.

Suárez, F., Aravena, J.E., Hausner, M.B., Childress, A.E. & Tyler, S.W. (2011). Assessment of a vertical high-resolution distributed-temperature-sensing system in a shallow thermohaline environment. *Hydrology and Earth System Sciences*, Vol.15, No.3, (March 2011), pp. 1081-1093, ISSN 1027-5606

Tyler, S.W., Burak, S.A., Mcnamara, J.P., Lamontagne, A., Selker, J.S. & Dozier, J. (2008). Spatially distributed temperatures at the base of two mountain snowpacks measured with fiber-optic sensors. *Journal of Glaciology,* Vol.54, No.187, (December 2008), pp. 673-679, ISSN 0022-1430

Tyler, S.W. & Selker, J.S. (2009). New user facility for environmental sensing, *EOS, Transactions, American Geophysical Union*, Vol.90, No.50, (December 2009), pp. 483, ISSN 0096-3941

Tyler, S.W., Hausner, M.B., Suárez, F. & Selker, J.S. (2009a). Closing the energy budget: advances in assessing heat fluxes into shallow lakes and ponds, *EOS, Transactions, American Geophysical Union*, Vol.90, No.52 (Fall Meet. Suppl.), ISSN 0096-3941, San Francisco, California, USA, December 2009

Tyler, S.W., Selker, J.S., Hausner, M.B., Hatch, C.E., Torgersen, T., Thodal, C.E. & Schladow, S.G. (2009b). Environmental temperature sensing using Raman spectra DTS fiber-optic methods. *Water Resources Research*, Vol.45, No.W00D23, (2009), 11 pp., ISSN 0043-1397

Turner, J.S. (1974). Double-diffusive phenomena. *Annual Review of Fluid Mechanics*, Vol.6, (January 1974), pp. 37-54, ISSN 0066-4189

Uchida, Y., Sakura, Y. & Taniguchi, M. (2003). Shallow subsurface thermal regimes in major plains in Japan with reference to recent surface warming. *Physics and Chemistry of the Earth,* Vol.28, No.9-11, (2003), pp. 457-466, ISSN 1474-7065

Vogt, T., Schneider, P., Hahn-Woernle, L. & Cirpka, O.A. (2010). Estimation of seepage rates in a losing stream by means of fiber-optic high-resolution vertical temperature profiling. *Journal of Hydrology,* Vol.380, No.1-2, (January 2010), pp. 154-164, ISSN 0022-1694

Westhoff, M.C., Savenije, H.H.G., Luxemburg, W.M.J., Stelling, G.S., van de Giesen, N.C., Selker, J.S., Pfister, L., Uhlenbrook, S. (2007). A distributed stream temperature model using high resolution temperature observations. *Hydrology and Earth System Sciences,* Vol.11, No.4, (2007), pp. 1469-1480, ISSN 1027-5606

Westhoff, M.C., Bogaard, T.A. & Savenije, H.H.G. (2010). Quantifying the effect of in-stream rock clasts on the retardation of heat along a stream. *Advances in Water Resources,* Vol.33, No.11, (November 2010), pp. 1417-1425, ISSN 0309-1708

Winograd, I.J., Landwehr, J.M., Coplen, T.B., Sharp, W.D., Riggs, A.C., Ludwig, K.R. & Kolesar, P.T. (2006). Devils Hole, Nevada $\delta^{18}O$ record extended to the mid-Holocene. *Quaternary Research,* Vol.66, No.2, (September 2006), pp. 202-212, ISSN 0033-5894

Yilmaz, G. & Karlik, S.E. (2006). A distributed optical fiber sensor for temperature detection in power cables. *Sensors and Actuators A: Physical*, Vol.125, No.2, (January 2006), pp. 148-155, ISSN 0924-4247
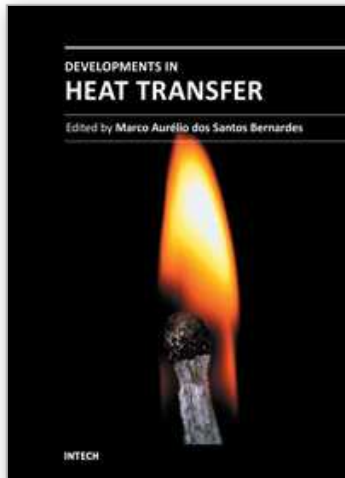
Developments in Heat Transfer

Edited by Dr. Marco Aurelio Dos Santos Bernardes

This book comprises heat transfer fundamental concepts and modes (specifically conduction, convection and radiation), bioheat, entransy theory development, micro heat transfer, high temperature applications, turbulent shear flows, mass transfer, heat pipes, design optimization, medical therapies, fiber-optics, heat transfer in surfactant solutions, landmine detection, heat exchangers, radiant floor, packed bed thermal storage systems, inverse space marching method, heat transfer in short slot ducts, freezing an drying mechanisms, variable property effects in heat transfer, heat transfer in electronics and process industries, fission-track thermochronology, combustion, heat transfer in liquid metal flows, human comfort in underground mining, heat transfer on electrical discharge machining and mixing convection. The experimental and theoretical investigations, assessment and enhancement techniques illustrated here aspire to be useful for many researchers, scientists, engineers and graduate students.

How to reference

In order to correctly reference this scholarly work, feel free to copy and paste the following:

Francisco Suárez, Mark B. Hausner, Jeff Dozier, John S. Selker and Scott W. Tyler (2011). Heat Transfer in the Environment: Development and Use of Fiber-Optic Distributed Temperature Sensing, Developments in Heat Transfer, Dr. Marco Aurelio Dos Santos Bernardes (Ed.), ISBN: 978-953-307-569-3, InTech, Available from: http://www.intechopen.com/books/developments-in-heat-transfer/heat-transfer-in-the-environment-development-and-use-of-fiber-optic-distributed-temperature-sensing